NJC

Accepted Manuscript

ROYAL SOCIETY OF CHEMISTRY

rsc.li/njc

View Article Online
DOI: 10.1039/C7NJ05138G

Synthesis, characterization and crystal structure of 2-chloroethyl (methylsulfonyl) methanesulfonate

J. E. Galván[1] M. E. Defonsi Lestard[1] O. E. Piro,[2] G. Echeverria,[2] R. D. I. Molina,[3] M.E. Arena,[3] S. E. Ulic,[4,5] M. E. Tuttolomondo[1*] and A. Ben Altabef[1]

[1]INQUINOA-CONICET, Instituto de Química Física, Facultad de Bioquímica, Química y Farmacia, Universidad Nacional de Tucumán, R. Argentina.

[2]Departamento de Física, Facultad de Ciencias Exactas, Universidad Nacional de La Plata and Institute IFLP (CONICET, CCT-La Plata), C. C. 67, 1900 La Plata, R. Argentina

[3]INBIOFAL-CONICET (Instituto de Biotecnología Farmacéutica y Alimentaria) Universidad Nacional de Tucumán, R. Argentina.

[4]CEQUINOR (CONICET-UNLP), Facultad de Ciencias Exactas, Universidad Nacional de La Plata, 120 N° 1465 (1900) La Plata, R. Argentina.

[5]Departamento de Ciencias Básicas, Universidad Nacional de Lujan, Ruta 5 y 7, 6700 Luján, Buenos Aires, R. Argentina.

Abstract

The aim of this work is to evaluate the structural, vibrational properties and the biological activity of 2-Chloroethyl (methylsulfonyl) methanesulfonate, $CH_3SO_2CH_2SO_2OCH_2CH_2Cl$ (Clomesone). The solid state molecular structure has been isolated and characterized by experimental (X-ray diffraction) and theoretical (DFT method) methodologies. The molecules are packed through C–H···O bifurcated interactions and Cl···Cl interactions. The experimental investigations were supplemented by quantum chemical calculation and Hirshfeld surface calculations. Furthermore, the infrared and Raman spectra for the solid phase have been recorded and the observed bands assigned to the vibrational normal modes. The study was completed by The Atoms-in-Molecules (AIM) theory and natural

View Article Online
DOI: 10.1039/C7NJ05138G

bond orbital (NBO) analysis. Finally, we study the function of Clomesone on biofilm formation and the study on a methansulfonate complex with respect to QS activity.

*Corresponding authors: Tel.: +54-0381-4311044; Fax: +54-3081-4248169; E-mail: *altabef@fbqf.unt.edu.ar*; *metdemunoz@yahoo.com*

Keywords: FTIR, Raman spectroscopies / crystal structure/ NBO calculations / DFT calculations.

View Article Online
DOI: 10.1039/C7NJ05138G

1. INTRODUCTION

The aim of the study is to characterize the crystal structure (X-ray diffraction, and Hirshfeld surface analysis) of 2-Chloroethyl (methylsulfonyl) methanesulfonate, $CH_3SO_2CH_2SO_2OCH_2CH_2Cl$ (Clomesone) besides determining its vibrational properties (FTIR, Raman).The characterizations of the structural and spectroscopic properties of Clomesone, was realized with the assistance of theoretical calculations. From these theory-experimental data identify the reactive sites of clomesone. The analysis of intermolecular interactions is focused particularly in O….H and Cl···Cl interactions since they play an essential role in the molecular self-assembly in crystals. For these reason the dimeric forms were modeled. Over the past years, the nature of Cl···Cl interactions were associated to specific attractive forces. They were justified in terms of the non-spherical shape of the halogen charge density, which caused a decrease in the exchange–repulsion interaction. Halogen bonds are the nature electrostatic with dispersion, polarization, and charge transfer due the electronic density of the halogen.[1-7]The stability of the different dimers in terms of hyper-conjugative and charge transfer interactions have been studied through the Second Order Perturbation Theory of the Fox Matrix by means of the NBO analysis.[8] The AIM theory[9] has been used to analyze the topology of all the optimized structures.

For several years it has been known that halo alkylating agents have antitumor activity since they produce cross-linking of the DNA strands. In particular, Clomesone, was evaluated in various types of animal tumors and compared to several agents. The results of such studies demonstrate that the antitumor activity of Clomesone is similar to that of the most effective alkylating agents.[10-17]

The activity of Clomesone against eukaryotic cells is well known. The compound is toxic to human cells[18] acts as antineoplastic drug[19]. However, the effect on bacterial biofilm was not determined. The biofilm is the predominant form in which bacteria is found in the environment and it is controlled by a chemical system of bacterial communication, called Quorum sensing (QS). Biofilms have been associated with non-malignant pathologies such as inflammatory bowel disease[20]. However, was determined that biofilms are associated with human colon cancer and linked to cancer location[21]. Biofilm emerged as an important factor in colorectal cancer initiation and progression[22]. In addition, Quorum sensing provides a unified model to explain many behaviors of tumor cells at all stages of cancer

View Article Online
DOI: 10.1039/C7NJ05138G

development.[23] Taylor et al.[24] suggesting that the metastasis formation could be mediated by a signaling circuit of quorum sensing type analogous to those previously identified in bacteria. For this reason, actually, knows cancer therapeutics are modified an assayed as anti-bacterial, anti-biofilm as well as anti-cancer efficacy.[25]

2. EXPERIMENTAL

2.1. Synthesis of 2-chloroethyl (methylsulfonyl) methanesulfonate

2-Chloroethyl (methylsulfonyl) methanesulfonate was prepared as reported in the literature[26] with slight modifications. In a round-bottom flask, 3mL of methanesulfonyl chloride dissolved in 3mL acetonitrile was added drop-wise under stirring to a solution of triethylamine (8 mL) and acetonitrile (17.5 mL). The mixture was kept at -30°C for 1 hour. After that, a solution of 2-chloroethanol (1.3 mL) in 1.3 mL of acetonotrile was added and stirred for two hours. The mixture was filtered at room temperature, to separate triethylamine hydrochloride and the solution was washed with NaCl 0.1M, dried over $MgSO_4$ and evaporated in vacuum to give an oil product (red oil). These oil was dissolved in a solvents mixture (dichloromethane:hexane) and stored overnight at -5ºC. The solid product was filtered, washed with cold hexane and recrystallized twice from hot chloroform. The obtained white crystalline solid was suitable for spectroscopic and structural studies.

2.2. X-ray data collection and structure refinement.

The measurements were performed on an Oxford Xcalibur, Eos, Gemini CCD diffractometer with graphite-monochromated CuKα (λ=1.54184 Å) radiation. X-ray diffraction intensities were collected (ω scans with ϑ and κ-offsets), integrated and scaled with CrysAlisPro[27]suite of programs. The unit cell parameters were obtained by least-squares refinement (based on the angular settings for all collected reflections with intensities larger than seven times the standard deviation of measurement errors) using CrysAlisPro. Data were corrected empirically for absorption employing the multi-scan method implemented in CrysAlisPro. The structure was solved by direct methods with SHELXS of the SHELX suite of programs[28] and the initial molecular model was refined by full-matrix least-squares procedure with SHELXL of the same package. The hydrogen atoms were positioned on stereo-chemical

View Article Online
DOI: 10.1039/C7NJ05138G

basis a refined with the riding model. The methyl H-atoms were refined as rigid groups allowed to rotate around the S-CH_3 bonds such as to maximize the sum of the observed residual electron density at their calculated positions. As a result, the –CH_3 group converged to a staggered conformation (**Tables S1-S4**).

2.3. Infrared and Raman spectroscopy

The FTIR spectrum was recorded in the 4000-400 cm^{-1} region with a spectral resolution of 2 cm^{-1} using a Perkin-Elmer GX1 FTIR spectrometer. The Raman spectrum of the solid was measured in the 4000–100 cm^{-1} interval with a Thermoscientific DXR Raman microscope. The Raman data were collected using a diode-pump, solid state laser of 532 nm. The resolution of the equipment employed was 1 cm^{-1}. A total of 64 scans were done in each condition and the spectra were analyzed using the OMNIC v.8.0 mathematical software provided by the manufacturer.

2.4. Computational details

The Gaussian 03[29] set of programs was used to carry out the DFT calculations. Full optimizations were performed with standard gradient techniques at the DFT levels of theory. Three types of basis sets were employed: Pople´s 6-31G(d), 6-311(3df) and 6-311++G**[30-34] basis sets were used. Becke's hybrid exchange B3[35] was the exchange functional, and the Lee–Yang–Parr non-local functional, LYP[36] was employed for correlation. In addition, Natural Bond Orbital (NBO) calculations were performed at the B3LYP/6-311G(3df) level of theory using the NBO 3.1 program.[37,38] AIM calculations were performed by means of AIM2000 program.[39] The atomic displacements given by the Gaussian program for each vibrational mode were used to understand qualitatively the nature of the molecular vibrations and, for that purpose; the corresponding data were represented graphically using the GaussView program.[40]

2.5. Hirshfeld surface calculations

Hirshfeld surfaces and their associated two-dimensional fingerprint plots[41-44] were obtained using CrystalExplorer 3.1 software[45] using the structural information obtained from X-ray diffraction. The d_{norm} (normalized contact distance) surface and the breakdown of two-

View Article Online
DOI: 10.1039/C7NJ05138G

dimensional fingerprint plots are used for decoding and quantifying intermolecular interactions in the crystal lattice.

The d_{norm} (normalized contact distance) surface and the breakdown of two-dimensional fingerprint plots are used for decoding and quantifying intermolecular interactions in the crystal lattice.

The *d*norm is a symmetric function of distances to the surface from nuclei inside and outside the Hirshfeld surface (di and de, respectively), relative to their respective van der Waals radii. 3D *d*norm surfaces are mapped over a fixed color scale of -0.08 au (red) – 0.6 Å au(blue), Shape index in the color range of –1.0 au (concave) –1.0 au (convex) Å, and Curvedness in the range of –4.0 au (flat) – 0.01 au (singular) Å. The 2D fingerprints plot are displayed by using the translated 0.6–2.6 Å range and including reciprocal contacts.

2.6. Bacterial growth

Overnight cultures of Pseudomonas aeruginosa PAO1, Pseudomonas aeruginosa PA14 and Staphylococcus aureus ATCC 6528 were diluted to reach an optical density (OD) of 0.125 ± 0.01 at 560 nm in Luria-Bertani (LB) and Müeller Hinton (MH) medium, respectively. The diluted culture (195 µL) was placed in one of the 96 wells of a microtitre polystyrene plate. Solutions of compound in dimethyl sulphoxide (DMSO, Sigma–Aldrich) were prepared separately, and 5 µl of each one was pipetted to the microtitre plate wells individually (5 replicates) to reach final concentrations of 200, 100, and 10 µg/mL.

Control wells (5 replicates) contained the diluted culture (195 µL) and 5 µL of DMSO, in which the final concentration of DMSO was 2.5%. Bacterial cultures were grown at 37°C for 24 h and growth was detected as turbidity (560 nm) using a microtitre plate reader (Thermo Fisher Multiscan Go, Finland). Ciprofloxacin was incorporated in the same bioassay as a positive control at 1 µg/mL.

2.7. Biofilm formation assay

For biofilm quantification, a micro method based on a protocol previously reported was employed.[46] The supernatants of bacterial cultures prepared as described previously, was discarded after 24 h incubation and the material that remained fixed to the polystyrene (containing biofilm) was washed with water. Biofilms formed were stained with 200 µL of

View Article Online
DOI: 10.1039/C7NJ05138G

an aqueous solution of crystal violet, (0.1% w/v) for 30 min. After washing with water, crystal violet bound to biofilm was removed from each, employing 200 µl of absolute ethanol and shaking for 30 min at 37°C with shaking. Absorbance (580 nm) of ethanol solutions of crystal violet was determined using the microtitre plate reader.

2.8. Biosensor assay

Detection of QS inhibition was carried out by a diffusion assay using the biosensor strain *Chromobacterium violaceum* CV026 Wells placed in the center of the surfaces of LB agar plates previously inoculated with *C. violaceum* CV026 and supplemented with 5 µg of the QS autoinducers, N-hexanoyl-L-homoserine lactone (HHL) (Sigma) were loaded with 50 µl of a 4 mg / mL solution of the compounds in DMSO to obtain 200 µg per well. DMSO was included as vehicle solvent control. After incubation for 18 h at 28 ° C, inhibition of QS was visualized by the presence of a clear halo on a violet background, where the presence of viable cells without the production of violacein around the well was disrupted.

The strains *C. violaceum* Tn5-mutant CV026 is unable to produce the pigment violacein per se, because it does not produce auto inducers. However, it is able to form violacein and its production depends on auto-inducer exogenous addition. [47]

The anti-QS compounds inhibit the production of violacein due to the antagonist molecules that bind instead of the natural autoinducers ligands and prevent the DNA from binding to the pigment transcription, considered an important virulence factor of *C. violaceum.*[48] In the *C. violaceum* CV026 bioassay, the presence of turbid halos on a violet background indicated QS inhibition without affecting microbial growth.

2.9. Statistical data analysis

All experiments were conducted in quintuplicates at least three times. Differences in the mean values were evaluated by analysis of variance (ANOVA). The Tukey test was used for all pair-wise multiple comparisons of groups. In all analyses, values of $p < 0.05$ were considered statistically different.[49,50]

View Article Online
DOI: 10.1039/C7NJ05138G

3. RESULTS AND DISCUSSION

3.1. Structural X-ray diffraction

Figure 1 is an ORTEP[51] drawing of the solid state molecule and intra/inter-molecular bonds distance and angles are in **Table 1.** These geometrical data for $CH_3SO_2CH_2SO_2OCH_2CH_2Cl$ molecule agree with Organic Chemistry's rules. Sulfur atoms acts with a six-valence bond capability showing S=O double bond distances in the range from 1.410(5) to 1.429(5) Å, S-C single bond lengths in the 1.746(8)-1.801(5) Å range, and d(S-O) = 1.566(4) Å. All carbon atoms show the expected sp^3 bonding structure with d(C-O) = 1.432(8) Å, d(C-C) = 1.475(8) Å, and d(C-Cl) = 1.775(8) Å. The molecule conformation is stabilized by intramolecular H-bonds, involving a C(1)-H(1A)···O(22) interaction [d(C···O)= 3.225Å, < C(1)-H(1A)···O(22)= 123.1°].

The optimized structural parameters of $CH_3SO_2CH_2SO_2OCH_2CH_2Cl$ were calculated like isolated and dimer structures at B3LYP method with different basis sets, these result are shows in **Table S5** in comparison with the experimental data with their RMSD corresponding. As a result, the dimer optimized parameters obtained by B3LYP/6-311G(3df) are in good agreement with experimental data. The deviation of dihedral angles C(2)S(2)O(3)C(3) and S(2)O(3)C(3)C(4) (approximately 20°) between the values of RX and those calculated for the monomer are corrected when calculating the dimer (~1°). This is because the geometry optimization of the dimer is performed considering the hydrogen bond interactions present in the crystal (**Table S6**).

The crystal structure is stabilized by strong intramolecular hydrogen bonds, resulting the strongest ones C(2)-H(2B)...O(12)#3 and C(3)-H(3B)...O(12)#3. This interaction is modeled by quantum methods as a dimer and the calculations show small deviations from X-ray structure.

View Article Online
DOI: 10.1039/C7NJ05138G

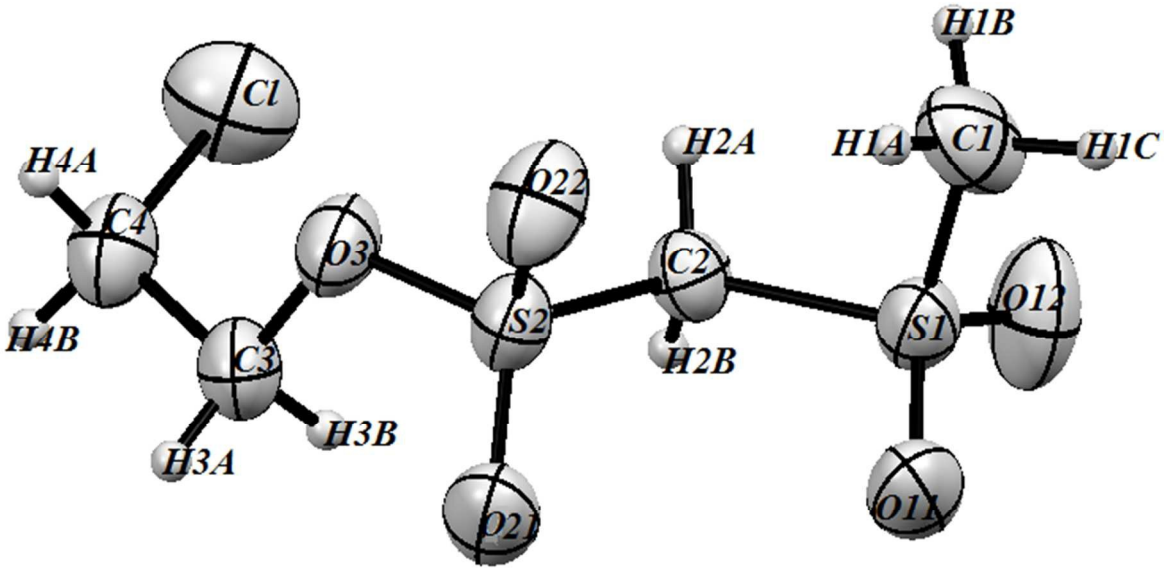

Figure 1. View of $CH_3SO_2CH_2SO_2OCH_2CH_2Cl$ X-ray structure showing the labeling of the non-H atoms and their displacement ellipsoids at the 30% probability level.

Table 1. Inter / intramolecular hydrogen bonds in the crystal structure of Clomesone.

X-Ray[a]	d(D-H)	d(H...A)	d(D...A)	<(DHA)
C(1)-H(1A)...O(22)	0.96	2.60	3.23(9)	123.1
C(2)-H(2B)...O(12)#3	0.97	2.28	3.17(9)	151.2
C(3)-H(3B)...O(12)#3	0.97	2.59	3.51(8)	158.7
C(1)-H(1B)...O(11)#1	0.96	2.41	3.19(1)	138.9
C(1)-H(1B)...O(21)#1	0.96	2.54	3.372(9)	144.4
C(1)-H(1C)...O(22)#2	0.96	2.61	3.314(8)	130.6
C(2)-H(2A)...O(21)#1	0.96	2.57	3.448(8)	150.9
C(3)-H(3A)...O(22)#4	0.97	2.66	3.305(7)	124.7

[a]Symmetry transformations used to generate equivalent atoms: (#1) x, y+1, z;
(#2) -x+1, y+1/2, -z+1; (#3) -x+2, y-1/2, -z+1; (#4) -x+1, y-1/2, -z

3.2. Hirshfeld Surface calculations

In **Figure 2** is observed a schematic view along b-axis, as bilayers. The Cl atoms are not involved in the hydrogen bonding and in each bilayer, chlorine atoms are arranged

View Article Online
DOI: 10.1039/C7NJ05138G

perpendicular to the b-axis and facing to each other at a distance of 3.7 Å(θCl···Cl···Cl = 95.8°). According to angular approach of halogens, the halogen-halogen interaction shave been classified as Type I (*cis* and *trans* geometry) and Type II (electrophile-nucleophile model or L- geometry). This interaction (θ1≈ 180°, θ2 ≈ 90°) represents a chemical model with each halogen atom polarized positively in the polar region and negatively in the other region. In the Clomesone crystal the bond angles are θ1=165.53°and θ2=75.26° around two Cl atoms (θC–Cl···Cl) therefore correspond to the Type-II interactions.[2]

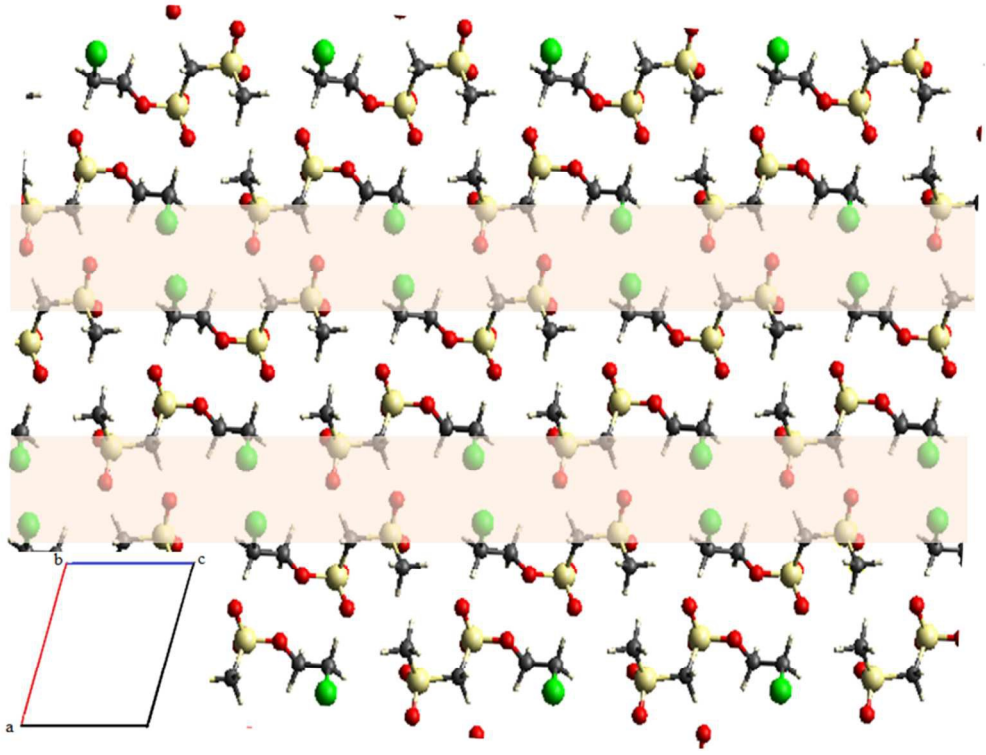

Figure 2. A view of packing diagram of $CH_3SO_2CH_2SO_2OCH_2CH_2Cl$

The bilayer is stabilized by Cl···Cl interactions and CH···O bifurcated interactions, leading to the formation of $R_2^1(7)$ rings stacked perpendicular to the *b*- axis (**Figure 3(A)**). In turn, the bi-layers stabilize each other by means of the H(1C)···O (22) interaction.

Figure 3(B) shows one of the sheets along a-axis, where the molecules are stabilized by bifurcated CH···OR interactions giving rise to the formation of 2 adjacent 6-membered rings ($R_2^1(6)$ and $R_1^2(6)$) arranged along the *b*-axis.

View Article Online
DOI: 10.1039/C7NJ05138G

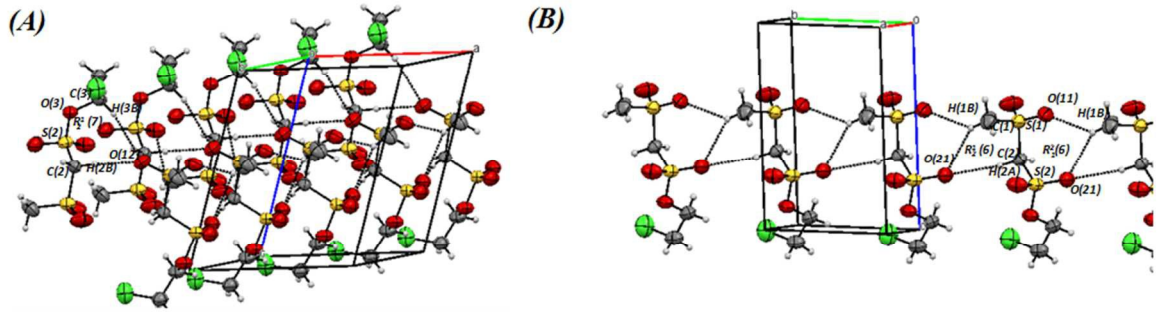

Figure 3. View of structure of $CH_3SO_2CH_2SO_2OCH_2CH_2Cl$: **(A)** along the *b*-axis and **(B)** along the *a*-axis.

The analysis of the Hirshfeld surface allowed to know the nature of the intermolecular interactions and their contributions to the crystal packing. The CH(2B)···O(12) and CH(3B)···O(12) hydrogen interactions (**Figure 4**(**A**)) are represented on the Hirshfeld surface as intense red color points (**Figure 4(B)).**

Hirshfeld surface analysis shows the highest proportion of H···O interactions (63.8%) and is displayed on the fingerprint plot with a blue circle (see **Figure 4**(**C**)).

The zigzag (**Figure 4**(**D**)) chain of Cl atoms observed in the crystal structure is displayed on the 2D-fingerprint plot as a bright streak circled in purple in Figure 4(C), representing only 1.2% of the surface. This low percentage does not reflect the strength and structure-directing effect that such an interaction has on the solid-state behavior of the molecule.

The contacts H ··H constitute 14.4% of the surface, with a short contact between a methyl proton and a methyl proton of a nearby molecule (2.77) Å, ∠= 118.4°, highlighted in black in **Figure 4**(**D**), giving rise a zigzag chain of CH_3 groups.

View Article Online
DOI: 10.1039/C7NJ05138G

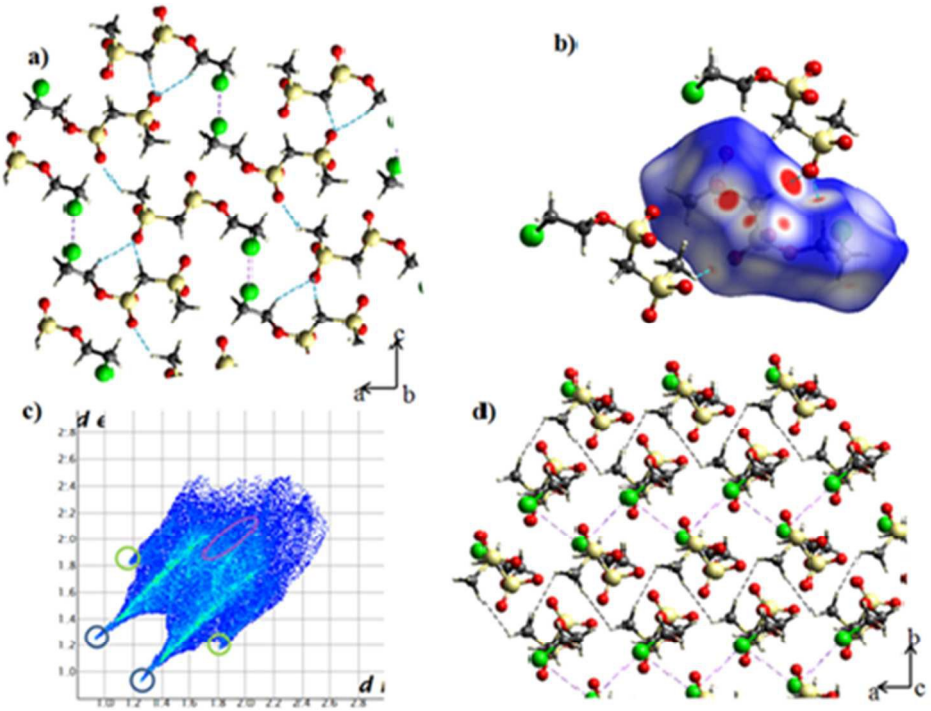

Figure 4. (a) Packing diagram with short contacts highlighted: Cl···Cl (purple), pair-wise O···H (blue). **(b)** CH(2B)···O(12) and CH(3B)···O(12) interactions are represented on the surface of Hirshfeld as intense red color points. **(c)** d_{norm} surfaces displaying the pair-wise O···H interaction. (**d**) Fingerprint plot with circled characteristic interactions: Cl···Cl (purple), O···H (blue), and H···H (black).

3.3. NBO analysis

Natural bond orbital (NBO) analysis has often been used in the evaluation of the anomeric effect and to explain the origin of the internal rotation barrier. The NBO analysis allows to estimate the energy of the molecule with the same geometry but in the absence of electronic delocalization. Moreover, only the steric and electrostatic interactions through E_{Lewis} are taken into account:

$$\Delta E = \Delta E_{Lewis} + \Delta E_{deloc.} \quad \text{(equation 1)}$$

where ΔE_{Lewis} represents the energy of the hypothetical localized species described by a determinant of nearly doubly occupied NBOs comprising the core electrons, lone pairs and

View Article Online
DOI: 10.1039/C7NJ05138G

localized bonds of the Lewis structure and the delocalization energy change, ΔE_{deloc}, represents the hyperconjugative stabilization contribution to the rotational barrier that arises from bond→antibond charge transfer.

Table 2. Calculated (B3LYP/6-311G(3df)]) contributions to the total energy of $CH_3SO_2CH_2SO_2OCH_2CH_2Cl$ from Lewis energy (E_{Lewis}), because of the localized electron density, and hyperconjugation energy (E_{deloc}) due to the delocalized electron density.

dimer	E_{total}[a]	ΔE_{total}[b]	E_{Lewis}[a]	ΔE_{Lewis}[b]	E_{deloc}[a]	ΔE_{deloc}[b]
$R_2^1(7)$	-3581.5427	0.00	-3577.5377	0.00	4.005	0.00
Cl···Cl	-3581.5389	9.96	-3577.9380	-1049.80	3.601	1060.5
$R_2^1(6)$	-3581.3104	609.21	-3577.3211	-568.04	3.989	41.3

[a] Absolute energies in Hartrees

[b] Relative energies in kJ mol^{-1}

NBO calculation in Clomesone was performed for dimers generated by intermolecular interactions: CH(2B)···O(12) and CH(3B)···O(12)($R_2^1(7)$); C(1)-H(1B)···O(21) and C(2)-H(2A)···O(21) (R6) and Cl···Cl at the B3LYP/6-311(3df) level of theory. **Table 2** presents the contributions due to the localized (E_{Lewis}) and delocalized (E_{deloc}) electron density for dimers of the crystal structure. The results show that the delocalization energy plays a significant role in the stabilization of $R_2^1(6)$ and $R_2^1(7)$ dimer and the electrostatic interactions for Cl···Cl dimer.

To complement the structural and conformational study of Clomesone, energy donor → acceptor interaction analysis was performed by approximating Natural Bond Orbital (NBO). For the $R_2^1(6)$ and $R_2^1(7)$ dimers stabilization, the electronic LP O → σ*C-H delocalization is greater for $R_2^1(7)$ than for $R_2^1(6)$, since the angles established in the hydrogen bonds of $R_2^1(7)$ (~ 160 °) allow a better superposition of the orbitals involved in the hyperconjugative interactions (**Table 3**).

The LPπO(3) → σ*C(2)-S(2) and LPπO(11/12) →σ*S(1)-C(1)/σ*S(1)-C(2) electronic delocalizations influence the value of the dihedral angles C(2)S(2)O(3)C(3) and C(1)S(1)

View Article Online
DOI: 10.1039/C7NJ05138G

C(2)S(2), respectively. These values correspond to *gauche* forms, characteristic of sulfonates and sulfones, where the mesomeric effect is responsible of the adopted structure. This behavior has already been reported for these systems.[52-54]

The largest delocalization in each unit of the dimer is caused by LPπO(21/22) → σ*S(2)-O(3) charge transfer, increasing the stability to the SO_2-O group. Therefore, these sulfonates are good groups of donors bound to SO2-O-, these results agree with the experimental results of Kenedy et al.[19] This group found that at pH values below the pKa of clomesone, the main degradation products were chloroethanol and (methylsulfonyl) methanesulfonate I produced by cleavage of a C-O bond instead of an S-O clomesone.[26,55] This delocalization is at its highest value for the Cl···Cl dimer (Table 3), which shows that the Cl ... Cl interaction is purely electrostatic but also due to the effect of polarization and dispersion that occurs in the electron density around the Cl.[2]

Table 3. Report of the most important hyperconjugative interaction contributions (kJ mol^{-1}).

Donor → Acceptor		$R_2^1(7)$	Cl···Cl	$R_2^1(6)$
LP σ O(3)	→σ*C(3)- C(4)	3.4	-	-
	→σ* S(2)-O(21)	13.5	15.1	13.4
	→σ* S(2)-O(22)	10.0	4.6	10.0
LPπO(3)	→σ* C(2)- S(2)	29.4	20.1	31.4
	→σ* C(2)- S(1)	6.5	6.0	5.9
	→σ* S(2)-O(21)	11.6	19.7	12.5
	→σ* S(2)-O(22)	7.4	-	7.4
	→σ*C(3)- C(4)	-	11.0	-
LP σ O(11/12)	→σ* S(1)-C(1)	3.4	3.0	0.8
	→σ* S(1)-C(2)	2.6	2.5	2.8
	→σ* S(1)-O(11/12)	4.9	5.5	4.4
LPπO(11/12)	→σ* S(1)-C(1)	77.0	72.2	84.0
	→σ* S(1)-C(2)	93.3	89.5	108.1
	→σ* S(1)-O(11/12)	92.4	88.3	96.4

View Article Online
DOI: 10.1039/C7NJ05138G

LP σ O(21/22) →σ* S(2)-C(2)	4.1	4.0	4.3
→σ* S(2)-O(21/22)	6.0	5.9	5.6
LPπO(21/22) →σ* S(2)-C(2)	86.0	80.3	95.2
→σ* S(2)-O(3)	126.9	126.5	130.4
→σ* S(2)-O(21/22)	88.0	85.9	90.2
LP σ O(11A) →σ*C(1)- H(1B)	-	-	2.51
LP σ O(21A) →σ*C(1)- H(1B)	-	-	0.63
LP σ O(21A) →σ*C(2)- H(2A)	-	-	0.88
LP π O(21A) → C(1)-H(1B)	-	-	1.55
LP π O(21A) → σ*C(2)- H(2A)	-	-	0.54
LPσO(12) →σ* C(2)- H(2B)	6.48		
→σ* C(3)- H(3B)	1.0		
LPπO(12) →σ* C(2)- H(2B)	5.4		
→σ* C(3)- H(3B)	3.1		

[a] LP is a lone pair on the specified atom. See Figure 1 for atom numbering.

[b]Calculated using the B3LYP/6-311G(3df) method

3.4. AIM analysis

One final attempt was made to rationalize the structure of Clomesone. Bader's Atoms-in-Molecules (AIM) quantum theory[9] has repeatedly shown to be helpful in bond characterization, through a topological analysis of the electronic charge density and its Laplacian at the bond critical point. The nature of the bonding interaction can be determined analyzing the charge density ρ(r) and its Laplacian $\nabla^2(\rho)$ at the bond critical point (BCP), and through the atoms properties, which are obtained integrating the charge density over the atomic basin. The results predict a stabilizing intramolecular bonding involving O(22) and H(1A)-C (1) and intermolecular contacts previously described as Cl···Cl and hydrogen bond type.

View Article Online
DOI: 10.1039/C7NJ05138G

Table 4. Local topological properties of the electron charge density (in au) at the bond, ring, and cage critical points in the intermolecular region for Clomesone.

Contact	Bond	ρ(r)	$\nabla^2(\rho)$	$\|V\|/G$	$\|\lambda_1\|/\lambda_3$	E_{int} (cal)
Intramolecular	C(1)-H(1A)...O(22)	0.00841	0.02926	0.832	0.1656	1.63
Intermolecular						
$R_2^1(7)$	C(2)-H(2B) ··O(12)#3	0.01199	0.04900	0.755	0.1680	2.33
	C(3)-H(3B) ··O(12)#3	0.00625	0.02238	0.772	0.1663	1.10
$R_1^2(6)$	C(2)-H(2A) ··O(21)#1	0.00615	0.02337	0.756	0.1625	1.11
	C(1)-H(1B) ··O(21)#1	0.00697	0.02630	0.761	0.1638	1.26
$R_2^1(6)$	C(1)-H(1B) ··O(21)#1	0.00697	0.02630	0.761	0.1638	1.26
	C(1)-H(1B) ··O(11)#1	0.00910	0.03712	0.739	0.1631	1.70
Cl···Cl	Cl···Cl	0.003141	0.00872	0.695	0.1494	0.36

Table S7 shows the properties of the electronic charge density in some selected BCP´s of the studied molecule. The values of ρ(r) and $\nabla^2\rho(r)$ for the C-C, C-S, S-O, C-H and C-Cl bonds are typical of a shared or covalent interaction, which is dominated by a contraction of ρ(r) towards the bond path, leading to its accumulation in the internuclear region. The ρ(r) values are within the (0.177 - 0.323) au range and $\nabla^2\rho(r)$ are in the (–0.130 - –0.860) au range.

Table 4 shows topological and energetic properties for six intermolecular and one intramolecular hydrogen bonds localized in the motive: ρ(r) and $\nabla^2\rho(r)$ values are in the (0.00625 - 0.01199) and (0.2238 - 0.04900) au ranges and are both positive being typical of weak hydrogen bonds. The charge density and Laplacian are within the range proposed by Koch and Popelier[56] for H-bond interactions that is 0.002–0.034 au and 0.024–0.139 au for charge density and Laplacian, respectively.

For Cl ··Cl interaction, the ρ(r) and $\nabla^2\rho(r)$ values are 0.003141 and 0.00872 au, respectively. Furthermore, the magnitudes of the kinetic energy density are greater than those of the potential energy density for all these interactions leading to $|V|/G < 1$ and $H > 0$,showing that these mainly electrostatic (δ+···δ−) interactions are very weak.

View Article Online
DOI: 10.1039/C7NJ05138G

The lower energy (E_{int}=1/2V) corresponds to the Cl ··Cl interaction and the higher to the C(2)-H(2B) ··O(12)#3 interaction of the R(7) ring.

3.5. Vibrational analysis

The experimental Raman and infrared spectra of $CH_3SO_2CH_2SO_2OCH_2CH_2Cl$ are shown in **Figure S1**. The observed and calculated wavenumbers, relative intensities and tentative assignment of fundamental vibration modes are given in **Table S8.** The experimental spectra were measured in solid phase, while calculated ones were performed as monomer and dimer at the B3LYP/6-311G(3df) level (**Figure 5).**

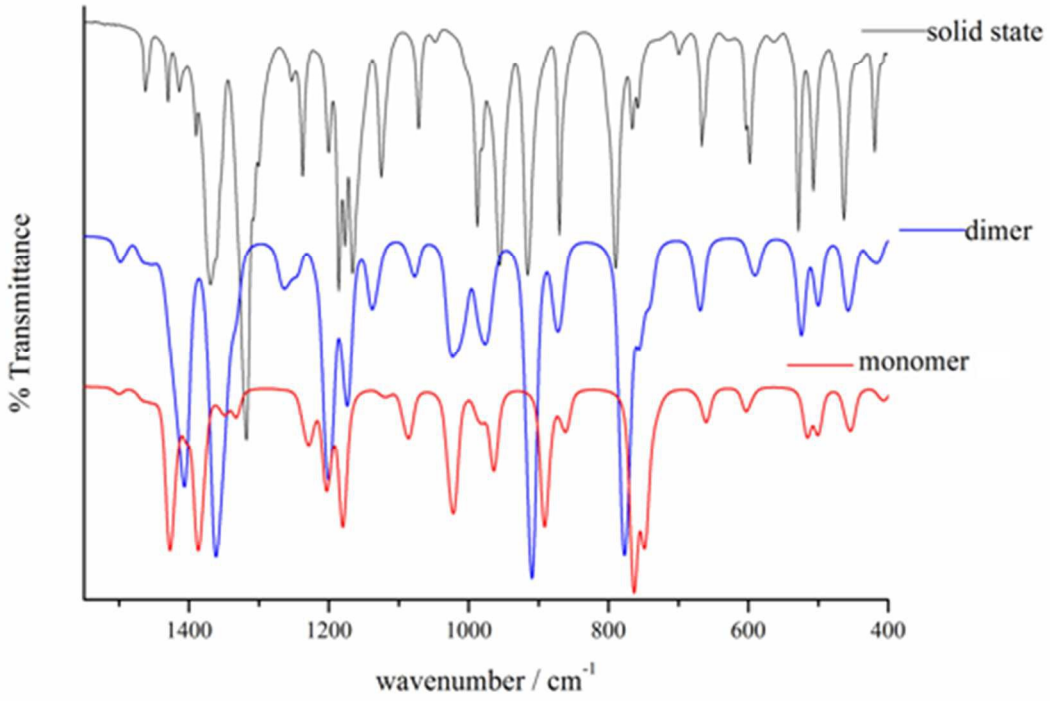

Figure 5. Infrared spectra of Clomesone between 1550 and 400 cm^{-1}: (upper trace) solid state; (resolution 2 $cm^{-1,}$ path length 10 cm^{-1}); calculated dimer (medium trace); calculated monomer (lower trace). The theoretical spectra are obtained from the frequencies (B3LYP/6-311G (3df)) calculated from the force field scales.

CH_3 modes. The bands at 3038 and 2938 cm^{-1} in IR and Raman spectra is assigned to the CH_3 asymmetric and symmetric stretching mode respectively. The weak intense bands at 1414 and 1390 cm^{-1} are assigned to the CH_3 asymmetric bending, while the symmetric

View Article Online
DOI: 10.1039/C7NJ05138G

mode is attributed to the medium band at 1301 cm^{-1}. The CH_3 rocking modes are assigned to the weak and the medium band at 982 and 956 cm^{-1}, respectively.

CH_2 modes. In the infrared and Raman spectra, the $C(2)H_2$ asymmetric and symmetric stretching modes appear at 3038 and 2990 cm^{-1}, respectively. The bands at 3022 and 2990 cm^{-1} are assigned to the $C(4)H_2$ asymmetric and symmetric stretching modes, respectively. (**Figure 6**) $C(3)H_2$ symmetric stretching mode can be attributed to the absorption at 2928 cm^{-1}. The CH_2bending modes are assigned at 1462 cm^{-1} ($\delta C(3)H_2$), 1430 cm^{-1} ($\delta C(4)H_2$) and 1361 cm^{-1} (δ $C(2)H_2$).The shoulders at 1354 and 1253 cm^{-1} are attributed to wagging of the $C(3)H_2$ and $C(4)H_2$ groups, respectively. The medium intense band at 1200 cm^{-1} is associated with the $\omega C(2)H_2$ mode. The twisting mode of the $C(3)H_2$, $C(4)H_2$ and $C(2)H_2$groups appear at 1237, 1186 and 1125cm^{-1}, respectively.

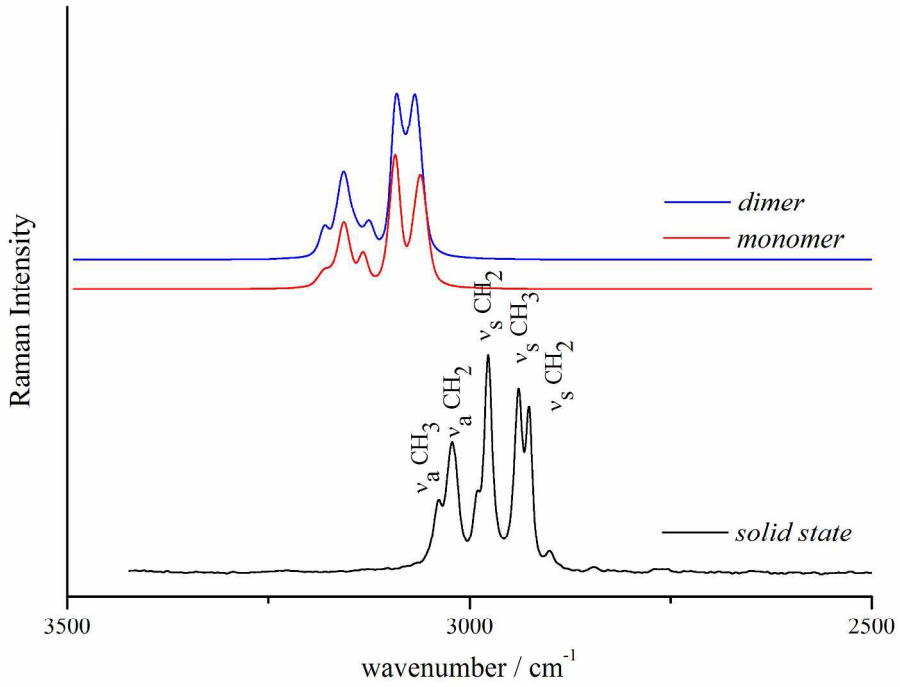

Figure 6. Experimental (lower trace) and theoretical Raman spectra (monomer and dimer) in the 3500-2500 cm^{-1} region.

View Article Online
DOI: 10.1039/C7NJ05138G

SO_2 modes.

Figure 7 shows the experimental and calculated infrared spectrum of the Clomesone in the stretching region of the SO_2 group. They are clearly observed four intense bands corresponding to both SO_2 groups present in the molecule, sulfonate ($S(2)O_2$) and sulfone ($S(1)O_2$). Two intense bands at 1370 and 1177 cm^{-1} are assigned to the ν $S(2)O_2$ asymmetric and symmetric modes, respectively. The very strong band at 1318 cm^{-1} and the intense band at 1166 cm^{-1} are assigned to the ν $S(1)O_2$ asymmetric and symmetric modes, respectively. At 1334 and 1187 cm^{-1} appear two weak absorptions that correspond to the asymmetric and symmetric stretching modes of S(1)O(12) ··H(2)-C(2) (Figure 7 - stars).

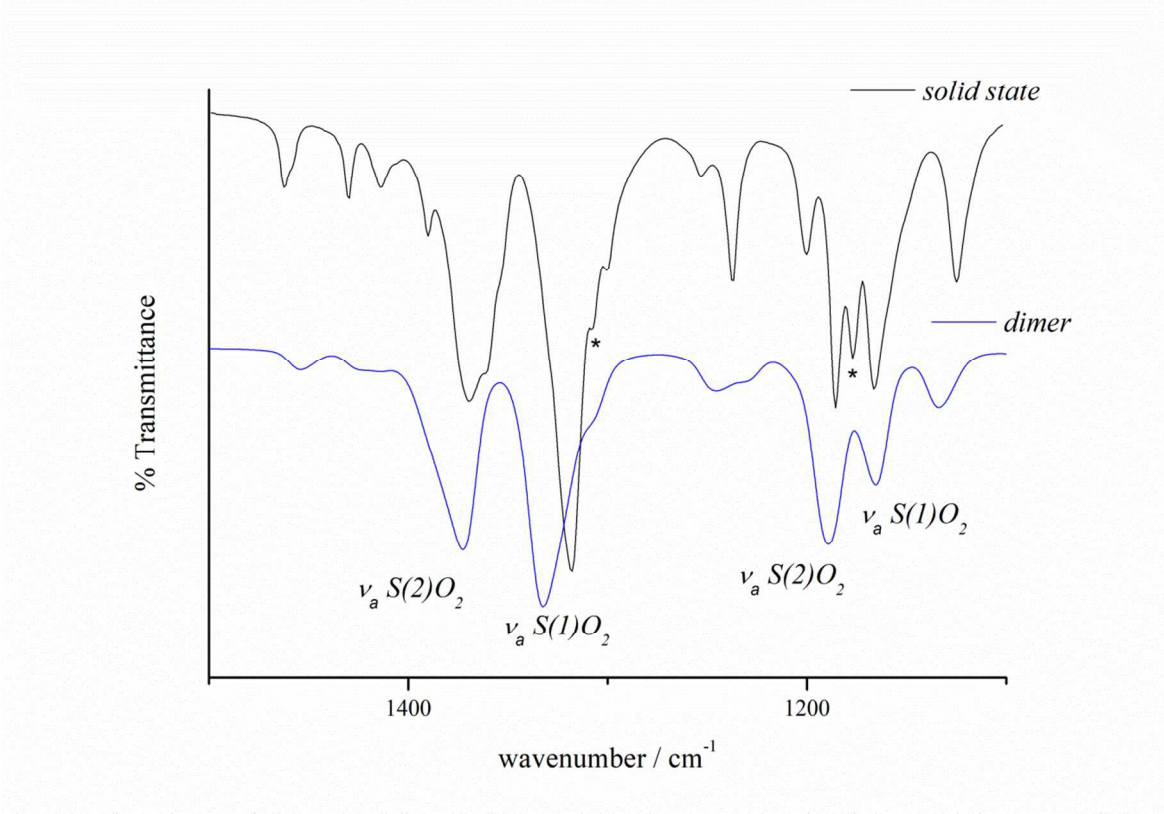

Figure 7. Experimental and theoretical infrared spectra in the 1500-1000 cm^{-1} region. The stars correspond to the asymmetric and symmetric stretching modes of S(1)O(12) ··H(2)-C(2).

The remaining bands corresponding to the vibrations of the whole $S(2)O_2$ group appear at relatively low frequencies: 598 cm^{-1} (wagging); 528 cm^{-1} (bending) and 352 cm^{-1} (twisting). Besides, the infrared bands at 507 cm^{-1} (bending), 464 cm^{-1} (wagging) and the Raman band

View Article Online
DOI: 10.1039/C7NJ05138G

at 271 cm^{-1} (twisting) are assigned to the $S(1)O_2$ group, which are also supported by computed and previous results.[52-55]

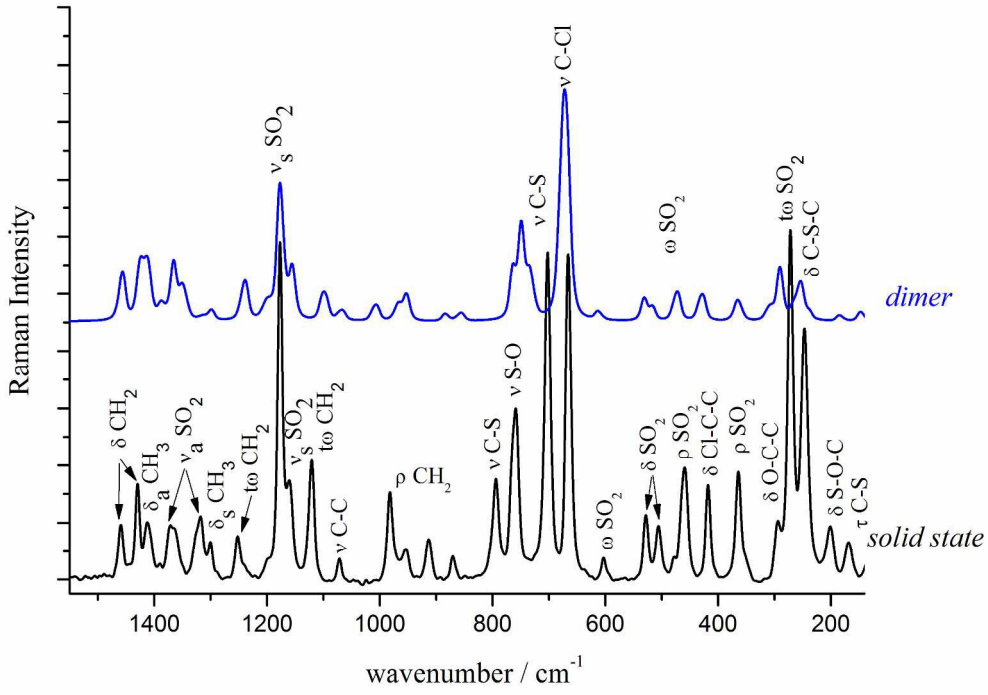

Figure 8. Experimental (lower trace) and theoretical (upper trace) Raman spectra in the 1500-100 cm^{-1} region.

Skeletal modes. The C(2)-S(2), C(1)-S(1),and C(2)-S(1) stretching modes are associated with the bands located at 790, 766 and 699 cm^{-1}, respectively. The medium band in the infrared spectrum at 667 cm^{-1} is assigned to the C(3)-Cl stretching. In addition, the C(3)-O(3), C(4)-C(3) and S(2)-O(3) stretching modes are located at 988, 1072, and 758 cm^{-1}, respectively (**Figure 8**).

3.6. Biological results

This is the first study on the methansulfonate complex different to the Colistinmethansulfonate (CMS), as well as the first study on a methansulfonate complex with respect to QS activity.

View Article Online
DOI: 10.1039/C7NJ05138G

The results showed that Clomesone is unable to inhibit the bacterial growth of *P. aeruginosa* or *S. aureus* in the range of assayed concentrations. However, it produces significant inhibition on the biofilm formation, mainly in *P. aeruginosa*. The biofilm formation of the strain of *P. aeruginosa* PAO1 diminished 63% in presence of 200 µg/mL of Clomesone and the inhibition of the strain PA14 was 22% at the same concentration. Considering that PAO1 and PA14 are the main studied strains for the biofilm inhibition due to their higher capacity to form biofilm with different strategies of virulence and since biofilm formation of both strains was inhibited by Clomesone, this suggests the possibility to use this compound as antipathogenic one.

Antipathogenic compounds do not kill bacteria or inhibit bacterial growth, but they rather control bacterial QS and biofilm formation, preventing the development of resistant strains.[57]

There is a linear correlation between growth inhibition and biofilm formation for *P. aeruginosa* strain PA14. Moreover, the biofilm inhibition was greater than the inhibition of bacterial development in the other two studied strains; indicating that Clomesone not only affects the growth but also the formation of biofilm (**Figures 9-11**).

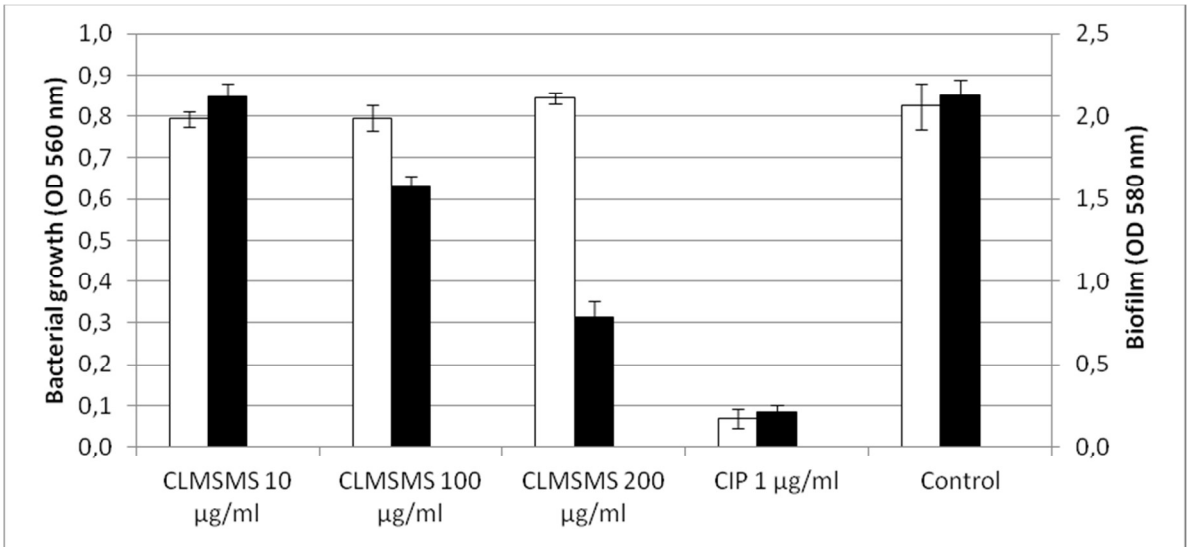

Figure 9: Growth (□) and biofilm production (■) by *P. aeruginosa* PAO1 cultures grown in LB broth in absence and presence of 10, 100, and 200 µg/mL of Clomesone. The

View Article Online
DOI: 10.1039/C7NJ05138G

inhibitor control used was CIP (Ciprofloxacin) 1 µg/mL. The error bars indicate standard deviation (n=8).

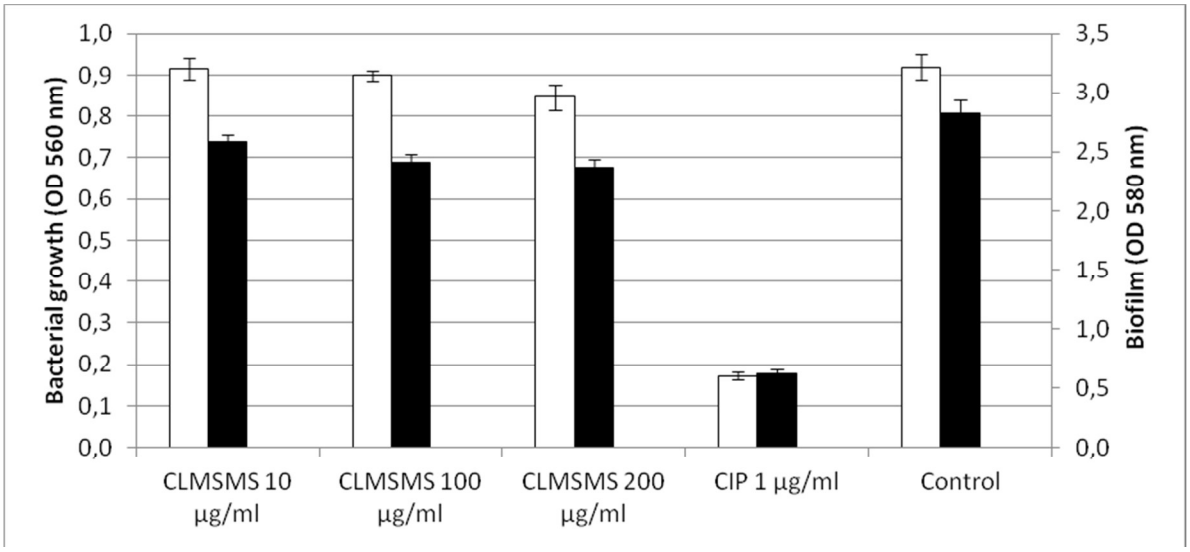

Figure 10: Growth (□) and biofilm production (■) by *P. aeruginosa* PA14 cultures grown in LB broth in absence and presence of 10, 100, and 200 µg/mL of Clomesone. The inhibitor control used was CIP (Ciprofloxacin) 1 µg/mL. The error bars indicate standard deviation (n=8).

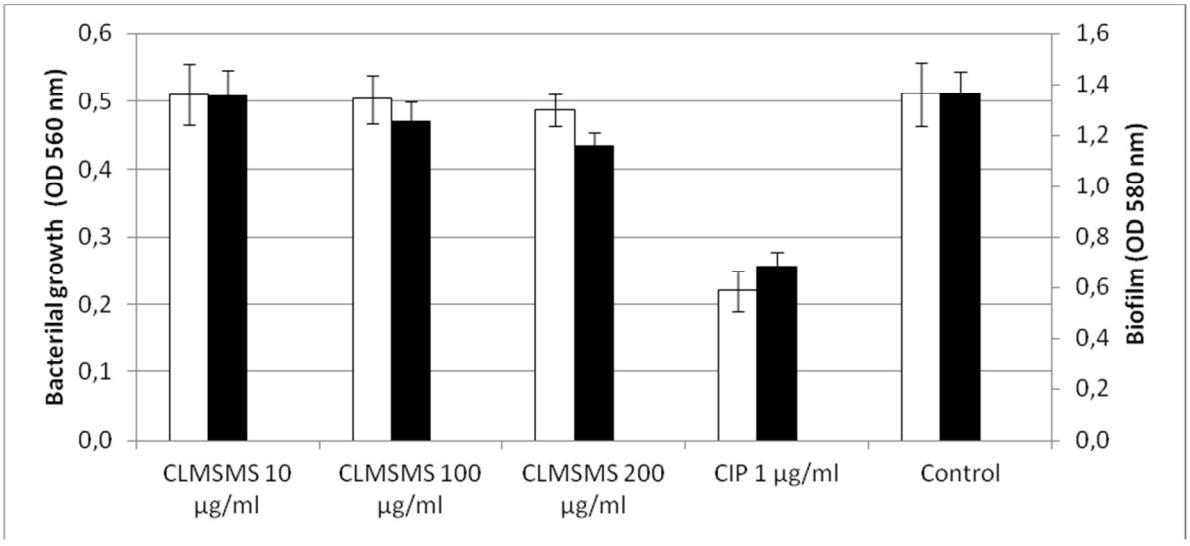

Figure 11: Growth (□) and biofilm production (■) by *S. aureus* cultures ATCC 6528grown in MH broth in absence and presence of 10, 100 and 200 µg/mL of Clomesone.

View Article Online
DOI: 10.1039/C7NJ05138G

The inhibitor control used was CIP (Ciprofloxacin) 1 µg/mL. The error bars indicate standard deviation (n=8).

According to the obtained results, the potential QS inhibitory effect of the compound was studied using the biosensor *Chromobacteriumviolaceum* CV026. The inhibition halo was 9.9 ± 0.5 cm for Clomesone and it showed bacterial growth indicating the QS inhibition (**Figure 12**). The observed decrease was significant and comparable with previously reported QS inhibitors at the same concentration.[58]

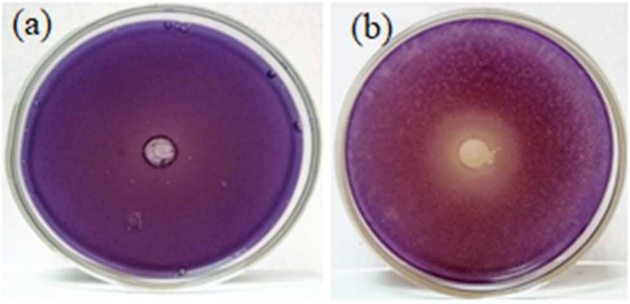

Figure 12. Competitive inhibition of violacein production induced by N-hexanoyl-L-homoserine lactone in *C. violaceum* CV026 by CLMSMS (b).Control (a)

A complex of methansulfonate is used for the administration of colistin. Colistin methansulfonate (CMS) is a prodrug that is hydrolyzed after intravenous administration to produce several derivatives, predominantly the active drug colistin. This complex is used to control *P. aeruginosa* colonization of the airway to prevent the pneumonia development because toxicity decreased significantly with respect to colistin.[50] This was the only methansulfonate complex previously studied with respect to biofilm target. The bactericidal effect of CMS on biofilm-forming cells of strain multidrug-resistant *P aeruginosa* was poor compared with those on the planktonic cells. These *in vitro* obtained results indicated that the efficacy of administered CMS depends on the resistance of the biofilm formed.[49]

View Article Online
DOI: 10.1039/C7NJ05138G

According to our results, Clomesone acts in the same way as CMS, inhibiting biofilm more than growth and its significant effect on biofilm could be explained by the QS inhibition.

The competitive inhibition of the Clomosone with HHL could be because they have similar electronic delocalization in their active sites. In addition, it was observed that Clomesone is more active than CMS although both have a sulfonate group in their structure.

At pH 5, Clomesone ionization takes place with the release of a chloroethyl cation and a highly electrophilic site in the sulfonate group. The greater biofilm inhibition´s ability of Clomosome compared to that reported for CMS, in spite of having the same active site (sulfonate group), it can be attributed to the different electronegativity of the environment. Besides, the much larger size of the CMS would be responsible of the low competitive inhibition with HHL due to steric hindrance (Figure S2), whereas that in Clomesone the active site where the autoinducer joins is favored due to its smaller size.

The stretching bands of the Clomesone sulfonate group are observed at 1370, 1177 and 758 cm^{-1} (assigned to ν_{as} S=O, ν_s S=O and ν S-O, respectively). These vibrational frequencies are suitable to characterize and identify Clomesone when it is part of a biological matrix. The band position of sulfonate group is directly related to the electronegativity of the neighboring groups. A greater electronic delocalization around this group turns it into a more attractive electrophilic site.[54]

CONCLUSIONS

2-chloroethyl (methylsulfonyl) methanesulfonate, Clomesone, was prepared as reported in the literature with slight modifications. Its solid state molecular structure was determined by X-ray diffraction methods. The crystal is stabilized by strong intermolecular H-bonds and Cl ··Cl interactions and the molecule conformation stabilized by an intra-molecular H-bonds. As this compound presents strong intermolecular H-bond interactions, the quantum chemical calculation was performed on its dimeric form. These computations were in very good agreement with the experimental results concerning both geometric and vibrational features.

View Article Online
DOI: 10.1039/C7NJ05138G

The delocalization in each unit of the dimer is produced from LPπO(21/22) →σ*S(2)-O (3) transition, stabilizing the SO_2-O moeity, this is the reason why these sulfonates are good donating groups attached to the SO_2-OR. These results are complemented by AIM study which predicts that the lower energy (Eint=1/2V) corresponds for the Cl ··Cl interaction and the higher to the C(2)-H(2B)...O(12)#3 interaction of the R(7) ring.

IR and Raman spectra were obtained for Clomesone and the vibrational data were used as a basis to perform an approximate description of the modes. The spectroscopic characterization of Clomesone results useful for its identification in pharmaceuticals and biological matrices and may be valuable in the standardization of Clomesone formulations, in pharmacokinetics studies, and potentially in therapeutic drug monitoring. In covalent sulfones, the SO_2 stretching modes are very sensitive to intermolecular hidrogen bonds.

In addition, Clomesone tests were performed with different biological media. The results showed that Clomesone is unable to inhibit the bacterial growth of *P. aeruginosa* or *S. aureus* in the range of assayed concentrations, but produces significant inhibition on the biofilm formation mainly in *P. aeruginosa*. The fact that Clomesone inhibits the mechanism of bacterial communication, *Quorum sensing,* analogous to the mechanism of metastasis formation, suggests the possibility of some other mechanism of action of this antineoplastic, which should be studied.

The greater biofilm inhibition of Clomosone suggests that sulfonate anion, remainig after ionization, is possibly the active group. This novel result supports that the spectroscopic characterization is fundamental in pure Clomosone, and the next target will be the spectroscopic characterization of the biological system.

Acknowledgements

The authors wish to thank Consejo de Investigaciones de la Universidad Nacional de Tucumán (CIUNT), Consejo Nacional de Investigaciones Científicas y Técnicas, PIP 002 and PIP 0359 (CONICET), ANPCyT (PICT2013- 0697), Universidad Nacional de La Plata (UNLP) and Departamento de Ciencias Básicas de la Universidad Nacional de Luján (UNLu) for financial support. S.E.U especially thanks Deutscher Akademischer Austauschdienst Germany (DAAD) for the FTIR spectrometer grant and financial support.

View Article Online
DOI: 10.1039/C7NJ05138G

Supporting Information available:

The supporting information includes:

Crystal data and structure refinement results for 2-chloro (methylsulfonyl) methanesulfonate **(Table S1);** Atomic coordinates (x 10^4) and equivalent isotropic displacement parameters (Å^2 x 10^3) for 2-chloro (methylsulfonyl) methanesulfonate. To be deposited **(Table S2);** Anisotropic displacement parameters (Å^2 x 10^3) for 2-chloro (methylsulfonyl) methanesulfonate. To be deposited **(Table S3);** Hydrogen coordinates (x 10^4) and isotropic displacement parameters (Å^2 x 10^3) for the 2-chloro (methylsulfonyl) methanesulfonate. To be deposited **(Table S4**);Theoretical and experimental geometric parameter of the Clomesone **(Table S5);** Theoretical Inter / intramolecular hydrogen bonds of the dimer form for Clomesone, calculated at B3LYP/6-311(3df) level **(Table S6);** Observed and Calculated Frequencies, Infrared and Raman Intensities for Clomesone **(Table S7**);Topological properties of Clomesone calculated at B3LYP/6-311G(3df) level (**Table S8);** Infrared and Raman spectra of Clomesone in solid state **(Figure S1)**. View of Clomesone, N-hexanoyl-L-homoserine lactone, $CH_3SO_2CH_2SO_2O^-$ and Colistin methansulfonate (CMS) **(Figure S2)**.

References

1 P. Politzer, J. S. Murray, T. Clark, *Phys. Chem. Chem. Phys*, 2013, **15**, 11178-11189.

2 M. V. Vener, A. V. Shishkina, A. A. Rykounov, V. G. Tsirelson, *J. Phys. Chem. A*, 2013, **117** (35), pp 8459–8467.

3 M. Capdevila-Cortada, J. Castelló, J. J. Novoa *CrystEngComm*, 2014, **16**, 8232–8242.

4 J. Trnka, R. Sedlak, M. Kolař, P.Hobza, *J. Phys. Chem. A,* 2013, **117**, 4331−4337.

5 S. Kozuch, J.M.L. Martin, *J. Chem.TheoryComput.*, 2013, **9**, 1918-1931.

6 G.M. Espallargas, F. Zordan, L.A. Marin, H. Adams, K. Shankland, J. van de Streek, L. Brammer, *Chem. Eur., J.* 2009, **15**, 7554 – 7568.

7 P.V. Gushchin, M.L. Kuznetsov, M. Haukka, V.Yu. Kukushkin, *J. Phys. Chem. A.,* 2013, **117**, 2827−2834.

8 A.E. Reed, R.B Weinstock, and F. Weinhold, J. Chem. Phys., 1985, **83**, 735-746.

View Article Online
DOI: 10.1039/C7NJ05138G

9 R.F.W. Bader, Atoms in and Molecules. A Quantum Theory, Clarendon Press, Oxford, 1990.

10 D. J. Dykes, W. R. Waud, S. D. Harrison, Jr., W. R. Laster, Jr., D. P. Griswold, Jr., Y. F. Shealy and J. A. Montgomery**,** *Cancer Research*, 1989, **49**, 1182-1186.

11 W. P Tong, K. W. Kohn and D. B. Ludlum, *Cancer Res.*, 1982, **42**, 4460-4464.

12 C. T. Combar, W. P. Tong and D. B. Ludlum, *Biochem.Pharmacol*, 1980, **29**, 2639-2643.

13 G. P. Wheeler, B. J. Bowden and R. F. Struck, *Cancer Res.*, 1975, **35**, 2974-2984.

14 N. W. Gibson, J. A. Hartley, J. M. Strong and K. W. Kohn, *Cancer Res.*, 1986, **46**, 553-557.

15 A. Pelfrene, S. S. Mirvish and B. Gold, *J. Nati. Cancer Inst.*, 1976, **56**, 445-446.

16 D. H. Swenson, J. V. Frei and P. D. Lawley, *J. Nati. Cancer Inst.*, 1979, **63**, 1469-1473.

17 H. E Kann, A. W. Prestayko, S. T. Crooke, L. H. Baker. S. K. Carter, and P. S. Schein, *New York: Academic Press, Inc.*, 1981, 95-105.

18 D. Y. Pacheco, L. R. Barrows, N. W. Gibson, *Journal of Cellular Pharmacology,* 1991, **2(2)**, 99-103.

19 Kennedy, P. E.; Riley, C. M.; Stella, V. J. International Journal of Pharmaceutics (1988), 48(1-3), 179-88.

20 A. Swidsinski, J. Weber, V. Loening-Baucke, L. P. Hale, H. Lochs, *J. Clin. Microbiol.*, 2005, **43**, 3380–3389.

21 C. M. Dejea, E.C. Wick, E. M. Hechenbleikner, J. R. White, J. L. Mark Welch, B. J. Rossetti, S. N. Peterson, E. C. Snesrud, G. G. Borisy, Lazarev, M., et al., *Proc. Natl. Acad. Sci. USA 111*, 2014, 18321–18326.

22 S. Li,S. R. Konstantinov,R. Smits, M. P. Peppelenbosch, *Trends in Molecular Medicine.* 2017, **23(1)**, 18-30.

23 M. Rivas Cañas Master Thesis.: Modelo multi-fase para el crecimiento tumoral en la fase avascular neoplásica: una hipótesis *quorum sensing* en los autoinductores tumorales. (Director Toni Guillamon i Grabolosa). Universitat Politecnica de Catalunya, Spain ,2009.

24 J. Taylor, V. Hiickson, T. Lotan et al , *Cancer Metastasis Rev.* 27:67-73, 2008.

View Article Online
DOI: 10.1039/C7NJ05138G

25 K. Laskar, S. Faisal, A. Raufa, A. Ahmed, M. , *Carbohydrate Polymers*, 2017, **166**, 14-23.

26 Y. Fulmer Shealy, C. A. Krauth, *Journal of Pharmaceutical Sciences,* 1993, **82(12),** 1200-1204.

27 CrysAlisPro, Oxford Diffraction Ltd., version 1.171.33.48 (release 15-09-2009 CrysAlis171.NET).

28 G. M. Sheldrick, *Acta Crystallogr*, 2008, **A64**, 112-122.

29 Gaussian 03, Revision C.01, M. J. Frisch, G. W. Trucks, H. B. Schlegel, G. E. Scuseria, M. A. Robb, J. R. Cheeseman, J. A. Montgomery, Jr., T. Vreven, K. N. Kudin, J. C. Burant, J. M. Millam, S. S.Iyengar, J. Tomasi, V. Barone, B. Mennucci, M. Cossi, G. Scalmani, N. Rega, G. A. Petersson, H. Nakatsuji, M. Hada, M. Ehara, K. Toyota, R. Fukuda, J. Hasegawa, M. Ishida, T. Nakajima, Y. Honda, O. Kitao, H. Nakai, M. Klene, X. Li, J. E. Knox, H. P.Hratchian, J. B. Cross, V. Bakken, C. Adamo, J. Jaramillo, R. Gomperts, R. E. Stratmann, O. Yazyev, A. J. Austin, R. Cammi, C. Pomelli, J. W. Ochterski, P. Y. Ayala, K. Morokuma, G. A. Voth, P. Salvador, J. J. Dannenberg, V. G. Zakrzewski, S. Dapprich, A. D. Daniels, M. C. Strain, O. Farkas, D. K. Malick, A. D.Rabuck, K. Raghavachari, J. B. Foresman, J. V. Ortiz, Q. Cui, A. G. Baboul, S. Clifford, J. Cioslowski, B. B. Stefanov, G. Liu, A. Liashenko, P. Piskorz, I. Komaromi, R. L. Martin, D. J. Fox, T. Keith, M. A. Al-Laham, C. Y. Peng, A. Nanayakkara, M. Challacombe, P. M. W. Gill, B. Johnson, W. Chen, M. W. Wong, C. Gonzalez, J. A. Pople, *Gaussian, Inc., Wallingford* CT, 2004.

30 W. J. Hehre, R. Ditchfield, J. A. Pople, *J. Chem. Phys.,*1972, **56**, 2257-2261.

31 P. C. Hariharan, J. A. Pople, *Theor. Chim. Acta,* 1973, **8**, 213-222.

32 M. S. Gordon, *Chem. Phys. Lett.,* 1980, ***76***, 3654-3665.

33 A. D. McLean, G. S.Chandler, *J. Chem. Phys.,* 1980, **72**, 5639-5648.

34 R. Krishnan, J. S. Binkley, R. Seeger, J. A. Pople, *J. Chem. Phys.,* 1980, **72**, 650-654.

35 M. J. Frisch, J. A. Pople, J. S. Binkley, *J. Chem. Phys.,* 1984, **80**, 3265-3269.

36 C. Lee, W. Yang, R. G. Parr, *Phys. Rev. B,* 1988, **37**, 785-789.

37 E.D. Glendening, J. K. Badenhoop, A. E. Reed, J. E. Carpenter and F. F. Weinhold, NBO 3.1 Theoretical Chemistry Institute, University of Wisconsin, Madison, WI, 1996.

38 J.P. Foster and F. Weinhold, J. Am. Chem. Soc., 1980, **102**, 7211-7218.

View Article Online
DOI: 10.1039/C7NJ05138G

39 F. Biegler-König and J. Schönbohm, AIM 2000 version 2.0, University of Applied Science, Bielefeld, Germany, 2002

40 B. Nielsen, A.J. Holder, GaussView, User's Reference; GAUSSIAN Inc.: Pittsburgh, PA, 1997–1998.

41 M.A. Spackman, D. Jyatilaka, *Cryst. Eng. Comm*., 2009, 11, 19-32.

42 M.A. Spackman, J.J. McKinnon, *Cryst. Eng. Comm*., 2002, 4, 378-392.

43 J.J.McKinnon, M.A. Spackman, A.S. Mitchel, *ActaCryst.. B,* 2004, **60**, 627–668.

44 J.J. McKinnon, D. Jayatilaka, M.A. Spackman, *Chem. Commun.,* 2007, 3814–3816.

45 S. K. Wolff, D. J. Green Wod, J. J. Mc Kinnon, M. J. Tuner, D. Jayactilaka, M. A. Packman. CrystalExplorer3.1 software University Western Australia. 2012

46 G. O'Toole and R. Kolter, *Molecular Microbiology*, **1998**, 28, 449-451.

47 K. H. McClean, M. K. Winson, L. Fish, A. Taylor, S.R. Chhabra, M. Camara, M. Daykin, J. H. Lamb, S. Swift, B.W. Bycroft, *Microbiology*, 1997, **143,** 3703–3711.

48 S. Manner, D. M. Goeres, M. Skogman, P. Vuorela and A. Fallarero. Sci. Rep., 2017, **7**, 1211-1222.

49 K. Marumo, D. Komukai, M. Hirose, H. Nakamura, H. Tanaka, K. Ugajin, G. Nagashima, Yoshimura, *J. Infect Chemother.,* 2013, **19,** 348–351.

50 R.L. Nation, J. Li, *Hodder Arnold*, 2010, 955-970.

51 L. J. Farrugia, *J. Appl. Cryst*., 1997,**30**, 565.

52 M.E. Defonsi Lestard, L.A. Ramos, M.E. Tuttolomondo, S.E. Ulic, A. Ben Altabef, *Spectrochim.Acta Part A: Molecular and Biomolecular Spectrosc.*, 2012, **96,** 332–339.

53 M.E. Defonsi Lestard, L.A. Ramos, M.E. Tuttolomondo, S.E. Ulic, A. Ben Altabef, *Vibrational Spectrosc.,* 2012, **59,** 40–46.

54 M. E. Tuttolomondo, A. Navarro, T. Peña, E. L. Varetti, S. F. Parker, A. Ben Altabef. *J. Phys. Chem. A,* 2009**, 113***,* 8401–8408

55 M. E. Tuttolomondo, A. Navarro, T. Peña, E. L. Varetti, A. Ben Altabef., *J. of Phys. Chem.A*, 2005, **109**, 7946 – 7956.

56 U. Koch, P. L. A. Popelier, *J. Phys. Chem.,* 1995, **99(24)**, 9747-9754.

57 M. Otto, *FEMS Microbiology Letters*, 2004, **241**, 135-141.

58 H. S. Vasavi, A. B. Arun, *Pharmacognosy Res*., 2015, **7(1),** 105–109.

View Article Online
DOI: 10.1039/C7NJ05138G

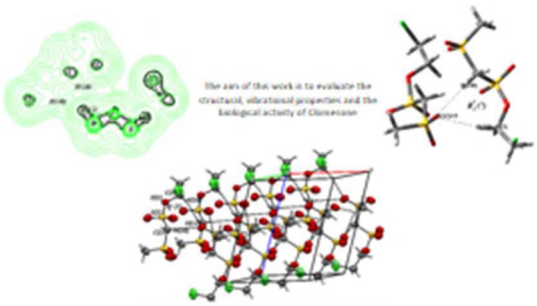

79x39mm (96 x 96 DPI)